Effect of different fiber combinations and optimisation of an ultra-high performance concrete (UHPC) mix applicable in structural elements

Kutalmış Recep Akça, Metin İpek [*]

Department of Civil Engineering, Sakarya University of Applied Sciences, Sakarya, Turkey

ARTICLE INFO

ABSTRACT

In this study, Ultra-High Performance Concrete (UHPC) mix was optimised to expand its use in large-scale applications. Using alternative curing methods instead of heat treatment, it was aimed that UHPC will meet the required strength and workability criteria and thus be presented applicable solutions for widespread use of UHPC in engineering applications. Therefore, effect of aggregate type, fiber content, curing method, compacting method, cement type, water/cement ratio and aggregate granulometry on mechanical properties of UHPC was investigated. Compressive strength, flexural tensile strength, splitting tensile strength, pull-out behaviour, modulus of elasticity and toughness values of the UHPC series were determined. Standard water curing (compared to wet hessian application) increased the compressive strength by 11.2% and the flexural tensile strength by 19%, while the inclusion of hybrid fibers (compared to the use of a single type of fiber) increased the compressive strength by 16.7% and the flexural tensile strength by 48%. Type of aggregate was found very effective on flexural tensile strength as well, and it provided additional ductility by increasing the matrix strength. In cases where heat treatment is not available, it was observed that the required strength criteria can be met with standard water curing as well. UHPC with a compressive strength of 170 MPa, which has excellent workability, was developed. As a result of the study, optimum solutions were proposed for the widespread use of UHPC in the precast industry.

1. Introduction

Ultra-High Performance Concrete (UHPC) is a new generation cement-based composite material with superior mechanical properties and durability. Although different values (100 to 120 MPa) were given in various standards [1–3], the minimum compressive strength of UHPC to be used in structural applications was stated as 150 MPa and 165 MPa for cylinder and cube specimens, respectively, in NF P 18-470 [4].

In recent decades, interest in high-strength materials is increasing in structural engineering applications, with the effect of the tendency towards slender, aesthetic and light structures. Owing to the ultra-high compressive strength of UHPC, the use of UHPC can reduce the weight of the structure to one third of a structure designed for the same purpose and with conventional concrete [5,6]. Due to the use of more slender elements and the decrease in the weight of the structure, UHPC reduces the earthquake load that will affect the structure, and also transportation and labor costs. In addition to it being used as an economical solution in large-span bridges, it is also seen as a potential material for wide use in high-rise buildings and protective structures (such as military buildings

and nuclear industry) [7–10]. Its superior durability provides a long service life with less maintenance [6].

UHPC has much higher compressive strength, tensile strength, fracture energy, durability, fatigue, impact and abrasion resistance compared to conventional concrete [10]. However, in order for UHPC to achieve the desired strength, it is generally recommended in the literature to apply heat treatment at 90 °C for at least 48 h [11–14]. Although it has numerous advantages over conventional concrete, the use of UHPC in engineering applications has remained limited due to the limited design codes (standards/guidelines) and the difficulty of performing heat/autoclave/steam curing in practice [15,16]. In addition to application difficulties, heat treatment application carried out for a long time is not preferred, as it is often seen as an additional cost and labor by the precast industry.

Graybeal [17] compared the compressive behaviour of untreated samples produced to simulate the potential condition that the large-scale structural element may encounter with steam-treated specimens. As a result of the study, it was shown that the compressive strength can be reduced by 35% if steam treatment is not applied. Moreover, it was

---

* Corresponding author.
E-mail addresses: akca@subu.edu.tr (K.R. Akça), metini@subu.edu.tr (M. İpek).

stated that the steam-treated samples behaved linearly up to 80–90% of compressive strength in stress–strain curves, whereas linearity was lost earlier in untreated specimens. In the study conducted by Shi et al. [18], a UHPC with a low carbon dioxide index was obtained by optimising the binder system. Thus, it was stated that an eco-efficient UHPC mixture was designed. As a result of the study, it was reported that the compressive strength of the UHPC mixture, which has a compressive strength of 201 MPa under autoclaved curing condition, is 150 MPa under standard curing. A study on the optimisation of UHPC mix was carried out by Chen and Zheng [19]. The highest compressive strength obtained under the standard water curing was reported as 129 MPa at cube specimens. However, it was stated that the mixes have extremely low fluidity due to the low water-to-binder (w/b) ratio and therefore it is difficult to cast into the mold. Zhang et al. [16] conducted a study on the enhancement of UHPC strength under standard water curing conditions with constant 3% fiber reinforcement. As a result of the study, it was reported that a UHPC with a compressive strength of 152.4 MPa was obtained from cube specimen with a w/b ratio of 0.194 and the collapse was 120 mm according to the conventional slump test. In another study investigating the effect of different curing conditions [20], it was stated that the consistency of fresh concrete was low enough to require additional operations such as hand operations and vibrators for casting and compaction, even though compressive strength up to 200 MPa was achieved with standard water curing. Nasrin and Ibrahim [21] investigated the mechanical properties of UHPC using locally available material as fine aggregate. It was reported that the compressive strength can be increased up to 55% with the appropriate choice of aggregates. In addition, it was stated that compressive strength of 140 MPa can be reached without applying any form of heat treatment. In the study conducted by Kazemi and Lubell [22], approximately 140 MPa compressive strength was obtained in the UHPC cube specimen under conventional moist curing. In the same study, the effect of the compacting method was also examined and 13% higher compressive strength was obtained from vibrated UHPC specimens compared to nonvibrated mixes. Dong et al. [12] compared the mechanical properties of standard cured and heat cured specimens. While the highest compressive strength obtained under standard curing conditions was 149 MPa, the importance of heat curing was pointed out at the end of the study.

Dingqiang et al. [23] proposed a mix design method for UHPC using various models. The effects of steel fiber on particle packing system were investigated by employing straight (long and short) and hooked-end steel fibers. As a result of the study, the fiber content was optimised using the D-optimal design (DOD) model and it was recommended that the fiber content should not exceed 2% for dense matrix structure and high fiber efficiency. On the other hand, several studies are available in the literature showing that mechanical properties improve as the amount of fiber increases [13,24,25], in addition to research that recommend the combination of short and long fibers [26,27]. Furthermore, flexural tensile strength increases both when the fiber alignment can be controlled and the fiber length increases [28]. Moreover, in order to obtain desired properties (such as strain-hardening behaviour accompanied by multiple micro-cracks), considerably high fiber content (i.e. 4–6%) could be required in UHPC [29]. However, considering that steel fibers constitute the majority of the cost of concrete, it is becoming more of an issue to study maximizing the strength by optimising the mixture, including minimizing the amount of fiber as much as possible.

Considering these, optimising the mix proportions is of great importance for the widespread use of UHPC. This study aimed to develop a UHPC that is well flowable and can be used in structural applications as well as meeting the required strength criteria without heat treatment by optimising the mix design of UHPC. Accordingly, in the first stage of the study, the effect of aggregate type, fiber content and curing type on UHPC's mechanical properties was experimentally investigated. For this purpose, different steel fiber contents were introduced into UHPC series that were manufactured using different aggregate types. After determining the optimum mix, the effect of alternative curing methods that can be applied to the structural element in case of not applying heat treatment on mechanical properties was investigated. In the second stage of the study, a series of experimental studies were carried out on improving the mechanical properties of the optimum mix. Thus, the effect of water-to-cement (w/c) ratio, compacting method, cement type and aggregate granulometry on mechanical properties was investigated experimentally. As a result of the study, optimum solutions have been proposed for the widespread use of UHPC in the precast industry, large-scale applications and structural element applications, thanks to the optimisation of mix proportions and simplification of the procedure followed in production.

2. Materials and method

2.1. Materials

Two types of Portland cement were used in the mixes. In addition to CEM I 52.5 N portland cement, which is widely used in UHPC, CEM I 42.5R was used in some series considering its widespread use in conventional concrete applications, ease of procurement and low cost. Moreover, undensified silica fume (SF) was used and chemical compositions of the binders are given in Table 1. 28-day compressive strengths of the cement were 52.9 MPa and 61.1 MPa for CEM I 42.5R and CEM I 52.5 N, respectively. Quartz powder (0–100 μm) and two types of sand as grain size were used in the mixtures. Sands with grain distribution of 100–300 μm and 300–700 μm were named as Sand-1 and Sand-2, respectively. Additionally, two types of sands having similar particle size distributions were used such as crushed quartz sand and natural silica sand. Table 2 provides the chemical composition and physical properties of the types of sands. Quartz sand is originally white in nature and iron content (Fe_2O_3) results in colours that range from pink to brown [30]. Thus, as seen in Table 2, natural silica sand containing relatively more Fe_2O_3 has light brown colour. A polycarboxylate-based highly active superplasticizer was used to achieve desired fluidity. This superplasticizer, in addition to fluidizing the fresh concrete, enables it to reach high strength in a short time [13]. Two types of steel fibers were used in the study. The brass-coated short straight fibers (6/0.2) and the long hooked-end fibers (35/0.75) are illustrated in Fig. 1 and their technical properties are given in Table 3. Particle size distribution of aggregates used in concrete series is shown in Fig. 2.

3. Method

3.1. Mixing

Pan type mixer with a capacity of 50 L was used to mix UHPC mixtures. However, due to the extremely low w/c ratio, the mixing method in UHPC is different from conventional concretes. Moreover, a wide variety of mixing methods are available for different UHPC mixes. Various researchers [13,24,31–33] have followed different methods of mixing UHPC mixes. The mixing procedure applied in this study was as follows:

- Binders (cement and silica fume) were put into the mixer and mixed dry for 3 min.
- Water and superplasticizer additive were slowly added to the mixture, allowing it to mix for another 7 min.
- Then, the rest of the dry components (powder and sand) were added into mixer and mixed for 4 min.
- Steel fibers were added last and allowed to mix for another 3 min until uniformly distributed.
- Mixing speed was kept constant throughout the mixing process.

Table 1
Chemical composition of the binders (%).

	SiO$_2$	Al$_2$O$_3$	Fe$_2$O$_3$	CaO	MgO	Na$_2$O eq.	SO$_3$	Cl$^-$	C$_3$S	C$_2$S	C$_3$A	C$_4$AF
CEM I 42.5R	19.8	4.7	3.18	64.35	1.27	0.77	2.49	0.008	67.80	5.62	7.08	9.68
CEM I 52.5 N	19.8	4.4	3.89	64.67	1.35	0.44	2.56	0.011	62.67	9.54	5.18	11.84
Silica Fume	94.1	0.7	0.25	0.50	0.60	0.56	0.50	0.10	–	–	–	–

Table 2
Chemical composition and physical properties of the sands (%).

	SiO$_2$	Al$_2$O$_3$	Fe$_2$O$_3$	CaO	MgO	Na$_2$O eq.	TiO$_2$	Colour	View
Crushed Quartz	99.5	0.01	0.01	–	–	0.37	0.07	White	
Natural Silica	98.3	0.91	0.20	0.02	–	0.07	0.12	Light Brown	

Fig. 1. Types of steel fibers used in the study.

3.2. Curing

In this study, it was taken into consideration that heat treatment, which will be applied for a long time, is not preferred by the precast industry, due to additional cost and labor reasons. Thus, instead of heat treatment, the traditional curing methods such as storing at 20 °C in water and covering with wet hessian (depending on the concrete series) were carried out until the experiment day, in accordance with the corresponding standard [34]. The curing methods used are illustrated in Fig. 3. All experiments were performed at the age of 28 days.

3.3. Optimisation of the aggregate granulometry

The aggregate combination used in the UHPC series manufactured in the first stage of the study was taken from the literature [13]. This aggregate mixture is hereinafter referred to as Aggregate Combination −1 (AC1). After the first stage, aggregate granulometry was optimised in order to examine the effect of aggregate granulometry on the mechanical properties of UHPC and to increase concrete strength. Thus, the

"Fuller and Thompson Curve" [35] was used. According to Fuller and Thompson, in case the aggregate gradation meet the reference curve obtained from Equation (1), the mix may have a better particle packing and thus higher compressive strength.

$$P = \left(\frac{d}{D_{max}}\right)^n x100 \tag{1}$$

where P is % finer than the sieve, d is aggregate particle size, D_{max} is maximum aggregate particle size, and n is a parameter that is taken 0.5 for maximum particle density.

With the help of the Fuller curve, a new aggregate combination denoted as AC2 was generated and was included in the experimental program since it was seen to be closer to the Fuller curve than AC1. In line with the scope of the study, in addition to the Fuller & Thompson curve, computer software was also used to enhance the compactness of the mix and obtain the denser particle packing. The mix proportions of the aggregate combinations that were obtained from literature, Fuller & Thompson equation and computer software are shown in Table 4. The aggregate ratios in Table 4 are given in proportion to the cement weight in the concrete mixture.

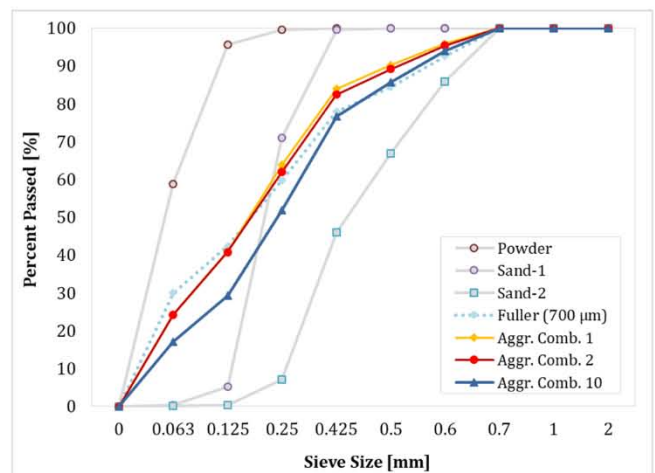In order to determine the aggregate combination having the highest

Fig. 2. Aggregates grading.

Table 3
Characteristics of the steel fibers.

	Length [mm]	Diameter [mm]	Aspect Ratio	Tensile Strength[MPa]	Modulus of Elasticity [GPa]	Shape
Short Fiber	6	0.20	30	≈ 2500	200	Straight
Long Fiber	35	0.75	45	≈ 1225	200	Hooked-end

Fig. 3. Curing methods.

Table 4
Proportions by weight to cement weight of aggregate combinations.

Notation	AC1	AC2	AC3	AC4	AC5	AC6	AC7	AC8	AC9	AC10	AC11	AC12
Powder	0.40	0.40	0.40	0.40	0.40	0.40	0.44	0.18	0.18	0.28	0.29	0.37
Sand-1	0.29	0.26	0.23	0.20	0.17	0.14	0.15	0.19	0.03	0.27	0.00	0.22
Sand-2	0.29	0.32	0.34	0.37	0.40	0.43	0.39	0.59	0.76	0.42	0.68	0.38
Source	Ipek et al., 2011	Fuller Curve	Computer Software									

compactness, the compacted bulk density values of all aggregate combinations given in Table 4 were experimentally analyzed (Fig. 4). Equation (2) was used to determine the compacted bulk density. Experimentally determined compacted bulk density values are shown in Fig. 4.

$$\Delta = \frac{W_{aggr.}}{V_{aggr.}} \qquad (2)$$

where Δ is compacted bulk density of the aggregate combination, $W_{aggr.}$ is the weight of the compacted aggregate combination and $V_{aggr.}$ is the volume of the aggregate combination.

It is seen in Fig. 4 that AC10 is the combination with the highest compactness among the combinations obtained from the computer software (i.e. 1.927 g/cm³). In addition to AC1 obtained from the literature and AC2 obtained from Fuller and Thompson equation, AC10 was selected among the combinations obtained from the computer software for the optimisation of aggregate granulometry and included in

the experimental program. Thus, three different aggregate combinations, AC1, AC2 and AC10, were used in UHPC productions. Particle size distributions of the aggregate combinations used in the scope of the study is shown in Fig. 2. When Fig. 2 is examined, it can be seen that AC2 is slightly closer to the Fuller reference curve than AC1. AC10, on the other hand, seems to be almost completely compatible with the reference curve, particularly in large grain sizes (i.e. d> ~ 400 µm), although it moves away from the reference curve in fine sieve sizes.

3.4. Experimental program

Within the scope of the study, many parameters such as fiber content, aggregate type, cement type, curing method, compaction method, aggregate granulometry, w/c ratio were investigated. In the first stage of the study, the effect of fiber content, aggregate type and curing method on UHPC mechanical properties in the series manufactured with the notation "Initial Mixes" (IM series) was examined. The mix proportions
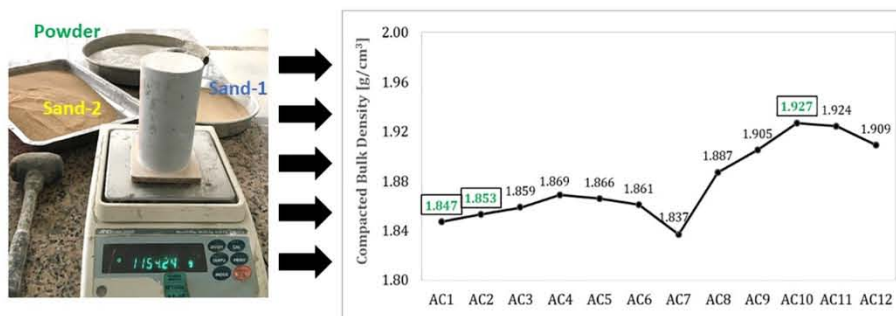

Fig. 4. Compacted bulk density values of the aggregate combinations.

of the IM series were taken from previous studies [13,36]. Crushed quartz sands (Sand-1 and Sand-2) were used at the initial stage of the research, and then replaced by natural silica sand which is locally more available. After determining the aggregate type that gives the best results in terms of mechanical properties, the effects of the two different curing methods were compared. Two types of fiber content were investigated in the research. While the short straight fiber content was kept constant at 2% by volume in some of the UHPC series, 2% short fibers and 1% long hooked-end fibers were combined in the rest. Thus, the fiber contents of 2% (straight) and 3% (2% straight + 1% hooked-end) by volume were investigated experimentally.

Once optimum fiber content, aggregate type and curing method were determined in terms of UHPC mechanical properties, the second stage of the study (with series M1 to M5) aimed to further improve the mechanical properties of the series which gave the best result. Therefore, after examining the effect of fiber content on different types of specimens (in cubic specimens unlike the IM series) in M1 series, the effect of cement type, compacting method, aggregate granulometry and w/c ratio on mechanical properties was investigated. Mix proportions and notations are presented in Table 5 and Table 6, respectively.

Two different compaction methods, vibrating table and internal vibrator, were used in different test series for compacting fresh concrete. Internal vibrator application was performed in one layer and two layers, respectively, in concrete series coded as M2-IV1 and M2-IV2. Taking into account the experimental findings w/c ratio was gradually decreased (0.25 to 0.20) in order to achieve the desired strength. The placement method used in the study was also effective in achieving this reduction. Additionally, the cement type was changed and aggregate granulometry was optimised to maximize the strength (in the second stage of the study).

The fluidity of UHPC was examined by flow table test in accordance with the standard [37]. Fresh UHPC was filled in a steel mold having a cone-shape, and then, allowed it to flow after the mold was lifted carefully. The flow table was dropped 25 times within a period of 15 s. Spread diameter was determined as an average diameter of perpendicular measurements. Thus, the minimum spread value obtained from the UHPC series was 215 mm (Fig. 5). This value that agreed well with the values reported by [8,38–40] can be assessed as well flowable.

In order to determine the compressive strength and modulus of elasticity, 100 × 200 mm cylindrical specimens were manufactured from IM series. Compressive strength in the final mixes (M1 to M5) was determined in cubic specimens (100 × 100 mm). When the final mix (M5) is obtained, both cubic and cylindrical specimens were manufactured for compressive strength, and the modulus of elasticity was determined in cylindrical specimens. Thus, the optimised UHPC mix (M5) was compared with the initial mixes (IM series), in terms of modulus of elasticity. In the compression tests, the loading rate was taken as 0.7 MPa/s in accordance with the standard [4].

Symmetrically arranged strain gauges were attached to the cylinder specimen surfaces using fast-setting cyanoacrylate type glue, in order to obtain stress–strain curves [4]. After the stress–strain curves obtained, modulus of elasticity values were calculated according to the standard [41], by using Equation (3).

$$E_c = \frac{0.4f_c - f_1}{\varepsilon_2 - 0.00005} \tag{3}$$

where f_c is the ultimate compressive strength, f_1 is the stress corresponding to a longitudinal strain of 0.00005, and ε_2 is the longitudinal strain produced by stress at 40% of f_c.

In order to determine the flexural tensile strength, prismatic specimens of 50 × 50 × 300 mm were manufactured and three-point bending test (Fig. 6a) was carried out. In addition to the flexural tensile strength, toughness values were also calculated for all series. Toughness values were calculated by using the area under the load–deflection curves up to 3 mm deflection. In order to determine the flexural tensile strength of the specimens, standard test procedure suggested by [42] was performed. In the final mix (M5) obtained as a result of the optimisation, prismatic specimens of specimen size (100 × 100 × 400 mm), which are widely used in the literature [43–46], were manufactured and four-point bending test (Fig. 6b) was performed. Thus, the flexural behaviour of M5, which is the final mix that was optimised, was examined in detail. Additionally, size effect was observed by comparing the flexural tensile strength of specimens manufactured in different sizes using the same mix.

In order to determine the splitting tensile strength of the final mix (M5), cubic specimens (100 × 100 mm) were manufactured, and standard test procedure suggested by GB/T 50081–2002 [47] was performed. Splitting tensile strength was calculated using Equation (4) suggested by [47], as in previous studies [48,49].

$$f_t = \frac{2P}{\pi A} = 0.637 \frac{P}{A} \tag{4}$$

where f_t is the splitting tensile strength, P is the splitting tensile failure load, and A is the area of split cross section.

In order to examine the adhesion of the steel fiber with the matrix, the pull-out test was performed in the M5 series. As soon as the UHPC mixture was placed in the cubic molds (100 × 100 mm), a single hooked-end fiber was centrally embedded into fresh mixture until half of the fiber length (i.e. $l_e = l_f/2$). 28 days after casting, single fiber was pulled out from the pull-out test specimens. The test speed was applied as 1 mm/min.

Table 5
Mix proportions UHPC series.

	CEM I 42.5							CEM I 52.5			
	Initial Mixes (IM)				Mix #1		Mix #2	Mix #3		Mix #4	Mix #5
	A	B	C	D	A	B	A	A	B	A	A
Cement:	1.00	1.00	1.00	1.00	1.00	1.00	1.00	1.00	1.00	1.00	1.00
Silica Fume:	0.30	0.30	0.30	0.30	0.30	0.30	0.30	0.30	0.30	0.30	0.30
Quartz Powder:	0.40	0.40	0.40	0.40	0.40	0.40	0.40	0.40	0.40	0.40	0.28
Sand-1:	0.29	0.29	0.29	0.29	0.29	0.29	0.29	0.29	0.26	0.29	0.27
Sand-2:	0.29	0.29	0.29	0.29	0.29	0.29	0.29	0.29	0.32	0.29	0.42
Water:	0.25	0.25	0.25	0.25	0.23	0.23	0.22	0.21	0.21	0.20	0.20
Steel Fiber (6/0.2):	0.18	0.18	0.18	0.18	0.18	0.18	0.18	0.18	0.18	0.18	0.18
Steel Fiber (35/0.75):	–	0.09	–	0.09	–	0.09	0.09	0.09	0.09	0.09	0.09
Superplast. (%):	3.00	3.00	3.50	3.50	3.00	3.00	3.00	3.00	3.00	3.00	3.00
w/c:	0.250	0.250	0.250	0.250	0.228	0.228	0.223	0.208	0.208	0.200	0.200
w/b:	0.192	0.192	0.192	0.192	0.175	0.175	0.172	0.160	0.160	0.153	0.153
Aggregate Comb.:	AC1	AC1	AC1	AC1	AC1	AC1	AC1	AC1	AC2	AC1	AC10

Table 6
Notations of the series.

Notation	Mix Proportion	Fiber Content	Sand Type	Curing Method	Compaction Method	Cement Type
IM-A-WH	Initial Mix A	2% Straight Steel Fiber	Natural Silica Sand	Wet Hessian	Vibrating Table	42.5
IM-B-WH	Initial Mix B	3% Hybrid Steel Fiber	Natural Silica Sand	Wet Hessian	Vibrating Table	42.5
IM-A-WT	Initial Mix A	2% Straight Steel Fiber	Natural Silica Sand	Water Tank	Vibrating Table	42.5
IM-B-WT	Initial Mix B	3% Hybrid Steel Fiber	Natural Silica Sand	Water Tank	Vibrating Table	42.5
IM-C-WT	Initial Mix C	2% Straight Steel Fiber	Crushed Quartz Sand	Water Tank	Vibrating Table	42.5
IM-D-WT	Initial Mix D	3% Hybrid Steel Fiber	Crushed Quartz Sand	Water Tank	Vibrating Table	42.5
M1-A	Mix #1A	2% Straight Steel Fiber	Natural Silica Sand	Water Tank	Vibrating Table	42.5
M1-B	Mix #1B	3% Hybrid Steel Fiber	Natural Silica Sand	Water Tank	Vibrating Table	42.5
M2-VT	Mix #2	3% Hybrid Steel Fiber	Natural Silica Sand	Water Tank	Vibrating Table	42.5
M2-IV1	Mix #2	3% Hybrid Steel Fiber	Natural Silica Sand	Water Tank	Internal Vibrator	42.5
M2-IV2	Mix #2	3% Hybrid Steel Fiber	Natural Silica Sand	Water Tank	Internal Vibrator	42.5
M3-A	Mix #3A	3% Hybrid Steel Fiber	Natural Silica Sand	Water Tank	Internal Vibrator	52.5
M3-B	Mix #3B	3% Hybrid Steel Fiber	Natural Silica Sand	Water Tank	Internal Vibrator	52.5
M4	Mix #4	3% Hybrid Steel Fiber	Natural Silica Sand	Water Tank	Internal Vibrator	52.5
M5	Mix #5	3% Hybrid Steel Fiber	Natural Silica Sand	Water Tank	Internal Vibrator	52.5

Fig. 5. Flowability test.

4. Results and discussion

4.1. Initial mixes (IM series)

Mechanical properties obtained from IM series can be found in Table 7. It was observed that standard water cured specimens (-WT coded) had higher strength than specimens covered with wet hessian (-WH coded) (both in terms of compressive and flexural strength). Considering this circumstance, standard water curing will be preferred for all specimens in the rest of the study, thus the modulus of elasticity values were determined only in the water-cured specimens. The standard water curing application increased the compressive strength by 4.9% and 11.2%, respectively, in specimens with 2% and 3% fiber content, while the flexural strength increased by 8.8% and 19%. In addition, it was observed that the series using natural silica sand have

better mechanical properties than the series using crushed quartz sand. Moreover, IM-C-WT series with the lowest compressive strength (i.e. 92.6 MPa) is not evaluated in UHPC strength class by some standards such as [3] due to compressive strength less than 100 MPa. When crushed quartz aggregate was replaced by natural silica sand, in the series containing 2% short straight fiber and 3% hybrid fiber, 18.5% and 16.4% higher compressive strengths were obtained, respectively, whereas an increase of more than 30% was obtained in flexural tensile strength. Moreover, regardless of aggregate type and curing method, when the fiber content increased, improvement in mechanical properties was observed in all UHPC series. Unlike conventional fiber-reinforced concretes, fiber reinforcement has a significant positive effect on the compressive strength of UHPC [13,24,50]. While the increase in fiber content (from 2% to 3%) led to an increase of about 16% in the compressive strength, it increased the flexural tensile strength up to 48%. In addition to total fiber volume, combining of different types of fibers influenced the mechanical properties of UHPC positively, as

Table 7
Mechanical properties of the initial mixes.

	Compressive Strength* (MPa) [St. Dev.]	Flexural Strength (MPa) [St. Dev.]	Toughness(kN. mm)
IM-A-WH	104.54 [2.44]	19.94 [0.13]	7.43
IM-B-WH	113.03 [3.85]	23.73 [0.85]	15.86
IM-A-WT	109.68 [1.23]	21.69 [0.19]	13.06
IM-B-WT	125.69 [3.05]	28.24 [1.37]	18.52
IM-C-WT	92.55 [1.34]	14.71 [0.45]	4.96
IM-D-WT	107.97 [1.76]	21.77 [0.48]	12.52

* Compressive strength value obtained from 100x200 mm cylindrical specimens.
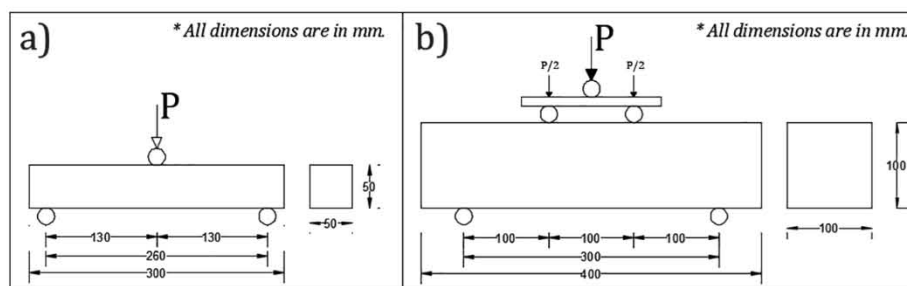

Fig. 6. Technical drawings of the flexural test mechanisms.

confirmed by [26,27,51]. Additionally, it is observed that flexural tensile strength increases when compressive strength increases. Due to the fact that changes in the series are reasonable, a considerably high correlation coefficient (i.e. 0.97) was obtained (Fig. 7).

Load-deflection graphs obtained from three-point bending tests are provided in Fig. 8. Appearance of the specimens after the experiment is shown in Fig. 9. Similar to the compressive strength, natural silica sand contributed positively to the flexural tensile strength as well. The use of natural silica sand indirectly increased the ductility of the UHPC mix, related to the increased strength of the concrete, due to the fact that debonding of the fibers became harder from the high strength matrix. Specimens manufactured from natural silica sand had the highest toughness when using 3% hybrid steel fiber, and failed after deflecting approximately 1/55 (L/55) of the span. A more brittle behaviour was observed in IM-C and IM-D series manufactured using crushed quartz sand, resulting in a L/154 and L/88 deflection. However, while short fibers control the cracks at the initial stage, macro cracks are formed and long fibers are activated as the load increases [26]. Thus, softening occurs faster in short-fiber reinforced concrete [52]. Therefore, specimens with 2% fiber content reached failure with less deflection. This circumstance reflected in the toughness results of the specimens. The series with the greatest flexural strength (i.e. 28.2 MPa) and toughness (i.e. 18.5 kN.mm) was the standard water cured IM-B-WT containing 3% hybrid steel fiber reinforcement and natural silica sand, while the lowest toughness values were obtained from the specimens having 2% micro fiber reinforcement. IM-B-WT was also able to continue to carry load linearly up to high load levels, as can be seen in Fig. 8. Furthermore, considering the post-peak stage, the use of long fiber in addition to the increased fiber volume is thought to have a positive effect on post-peak ductility. Accordingly, it was observed that the slope of the descending branch was generally smaller in specimens with 3% hybrid fiber content. While post-cracking behaviour depends on fiber content, geometry and orientation, increasing the length of steel fibers significantly increases the strength and fracture energy after cracking [53,54].

Additionally, multiple cracking and deflection hardening are some of the distinctive properties of UHPFRC as a cement-based composite material having outstanding mechanical properties, ductility, and durability [52,55]. Particularly in IM-B-WT, with the indirect contribution of the aggregate used in addition to the high fiber content, multiple cracking was observed before deformation started to localize in the decisive failure crack (Fig. 10). Although in the other UHPC series, when the crack formed perpendicular to the plane of the specimen in the midpoint of the span is generally decisive, it was observed that the secondary crack formed perpendicular to the specimen plane in the middle of the span in IM-B-WT and could not reach up to the bottom of the cross section (Fig. 9). Additionally, the path that is followed by the crack was extended, owing to its high fiber content. It is thought that the
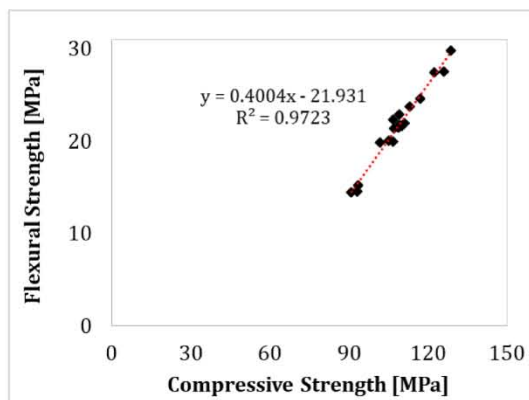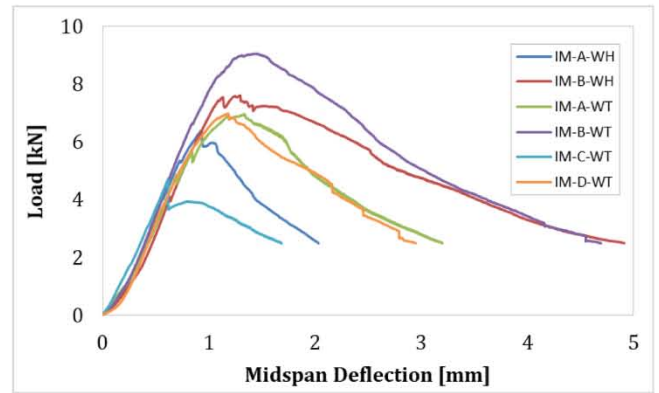

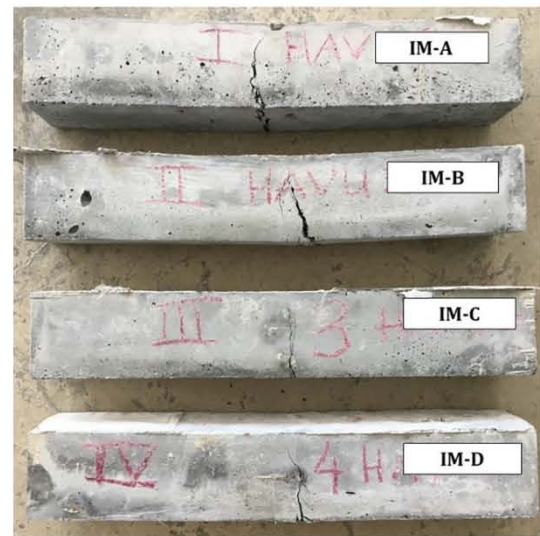**Fig. 8.** Load-deflection curves of the initial mixes.

Fig. 9. Prism specimens after bending test.

orientation of the crack towards the section where the fiber orientation is favorable for itself has a positive effect on the UHPC performance under bending (Fig. 10).

4.2. Final mixes (M series)

Mechanical properties obtained from the final mixes can be found in Table 8. Depending on the increase in fiber content, a 14.8% improvement, which is in agreement with the cylindrical specimens of IM series, was observed in the compressive strength of the cube specimens. While 2% short straight fiber-reinforced M1-A has a compressive strength of 113.6 MPa, its compressive strength increased to 130.4 MPa with 3% hybrid fiber content. By taking into account this finding, 3% hybrid fiber inclusion was adopted for the rest of the study. In the M2 series, where the effect of compaction methods on mechanical properties was examined, it was observed that the application of internal vibrator in two layers (denoted as M2-IV2) contributed significantly to the compressive strength. Due to the small section height, the internal vibrator could only be applied in one layer and therefore bending specimens were not manufactured from M2-IV2.

When the w/c ratio was reduced from 0.21 to 0.20, the compressive strength increased by 5%, while a significant change was not observed in the flexural tensile strength and toughness values. The experimental study began with CEM I 42.5 cement, which is the most widely used in conventional concrete manufacturing, taking into account the convenience of storage and supply. However, since the desired strength could
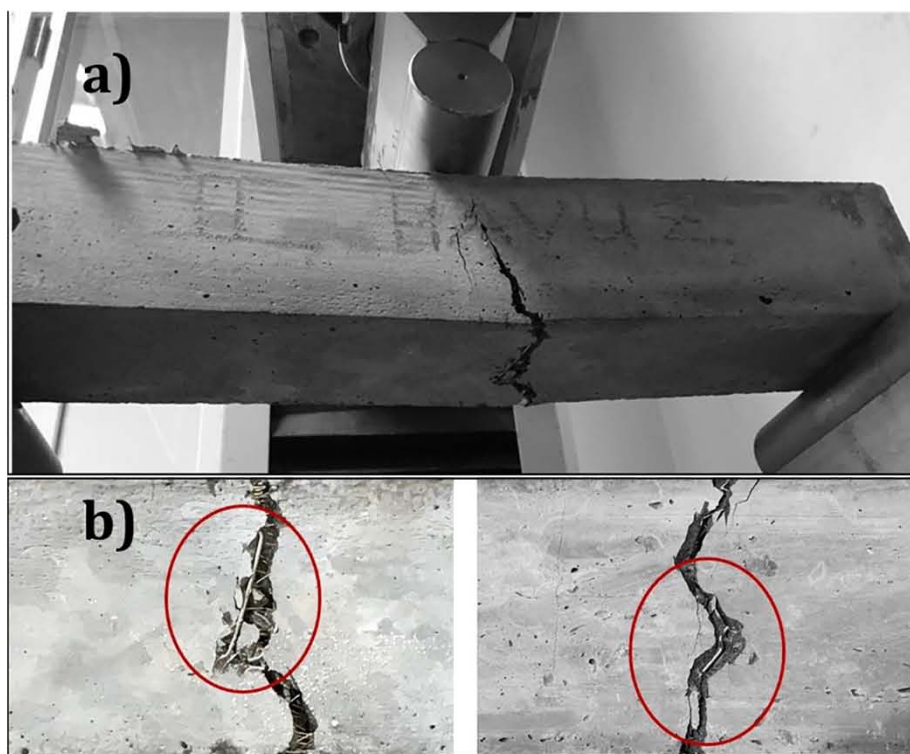

Fig. 7. Correlation of compressive strength and flexural tensile strength (for initial mixes).

Fig. 10. Crack formations on specimens (a) general view (b) bottom view.

Table 8
Mechanical properties of the final mixes.

	Compressive Strength* (MPa) [St. Dev.]	Flexural Strength (MPa) [St. Dev.]	Toughness(kN. mm)
M1-A	113.56 [4.41]	18.89 [0.17]	7.46
M1-B	130.41 [4.62]	21.12 [0.58]	12.11
M2-VT	125.28 [1.44]	21.33 [0.47]	8.57
M2-IV1	114.69 [3.94]	16.08 [0.79]	8.42
M2-IV2	135.16 [3.01]	–	–
M3-A	158.11 [2.61]	23.73 [0.80]	13.05
M3-B	154.05 [2.81]	19.42 [0.53]	9.84
M4	165.92 [1.77]	23.18 [0.38]	14.73
M5	170.34 [1.19]	25.29 [0.19]	14.38

* Compressive strength value obtained from 100x100 mm cubic specimens.

not be achieved, CEM I 52.5 was used by changing the cement type in Mix # 3 and subsequent mixes. When the cement strength increased, the compressive strength of UHPC also increased, as expected. When the cement type was changed and w/c ratio was reduced (from ~0.22 to ~0.21), an increase of approximately 17% was observed in the compressive strength. However, in the M3 series where the high strength cement (CEM I 52.5 N) is used, large air voids ($D_{void} \approx 6.9$ mm) were detected on the concrete surface after the compression test (Fig. 11a). The diameters of the voids seen in Fig. 11a vary between 3.5 and 6.9 mm. It is thought that these spherical voids, which are independent of each other, are formed by the effect of the superplasticizer. These voids should be minimized, in order to increase the concrete strength. Although the same compaction procedure was applied in fresh state, it was observed that the number and the size of the voids decreased (i.e. $D_{void} \approx 2.6$ mm) in the M5 series (Fig. 11b). In addition to reducing the w/c ratio, optimising aggregate granulometry is thought to be effective in minimizing these voids. Optimising aggregate granulometry and using the densest aggregate combination (AC10) obtained by using

computer software created a more compact structure. The minimization of the voids led to increases in the compressive strength as well. The highest compressive strength was obtained from M5 with 170.34 MPa. Thus, the strength (at least 165 MPa in cube specimen), which is given in the French code [4] and aimed to be achieved in this study, was exceeded.

Load-deflection graphs obtained from three point bending tests are reported in Fig. 12. The use of high-strength cement, although not as aggressive as it is in compressive strength, has also positively affected the flexural tensile strength. Additionally, optimisation of aggregate granulometry also led to a 9% increase in flexural tensile strength. By means of the optimisation of the granulometry, a more compact mix was obtained (Fig. 4). This circumstance, besides the increase in compressive strength, is thought to make fibers debonding difficult from the matrix. Fibers that cannot be easily debonded from a matrix with high compactness and strength increased the flexural tensile strength, resulting in the increased the crack bridging they make. Similar to the compressive strength results, it was seen that the M5 series has the highest flexural tensile strength. When the maximum deflection values of the specimens at the time of failure are compared, it was observed that the largest deflection (i.e. ~4.5 mm) was obtained from the M4 and M5 series, while M2-VT (compacted using vibrating table) and M1-A (having 2% fiber content) series failed without large deflections after peak load. This circumstance reflected in the toughness results of the specimens as well. Thus, the greatest toughness values were observed at M4 and M5. Additionally, it can be stated that the initial stiffness of the series having the same fiber content may vary slightly depending on the compressive strength. Moreover, all specimens continued to carry load after the first crack and exhibited deflection hardening behaviour.

It is observed that flexural tensile strength increases when compressive strength increases as is the case with the initial mixes. In other words, there is a parallel manner between compressive strength and flexural tensile strength as seen in Fig. 13. However, a lower correlation coefficient (i.e. $R^2 = 0.63$) was obtained from the final mixes than that of IM series (i.e. $R^2 = 0.97$), due to the variability of w/c ratio and the use of cement with different strength. This can be explained by
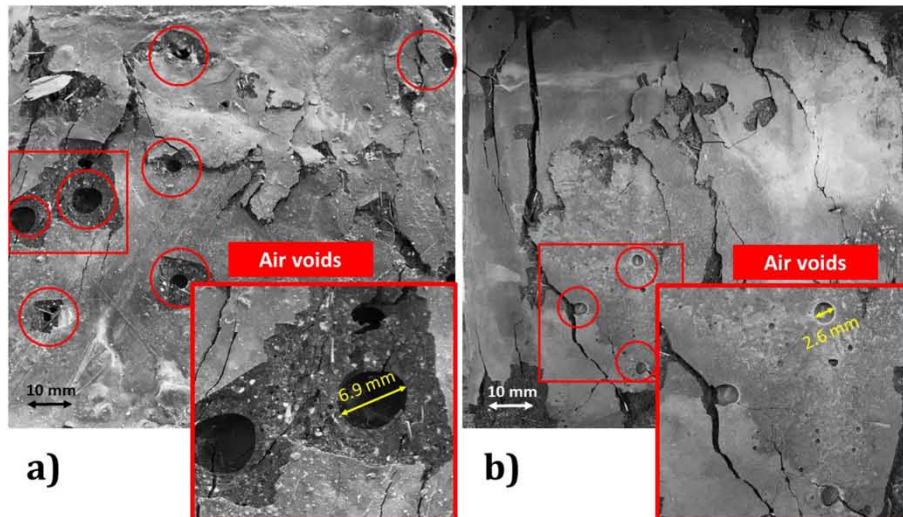
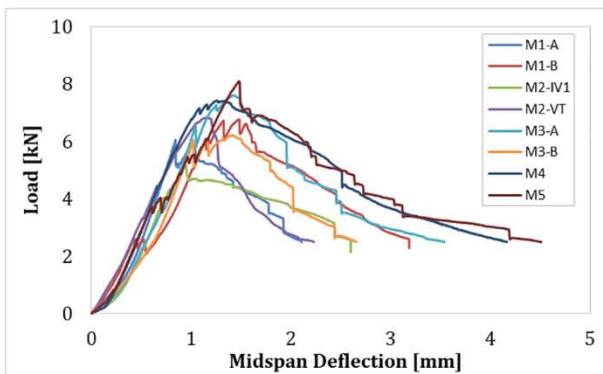**Fig. 11.** Air voids on specimens surface (a) M3-A (b) M5.

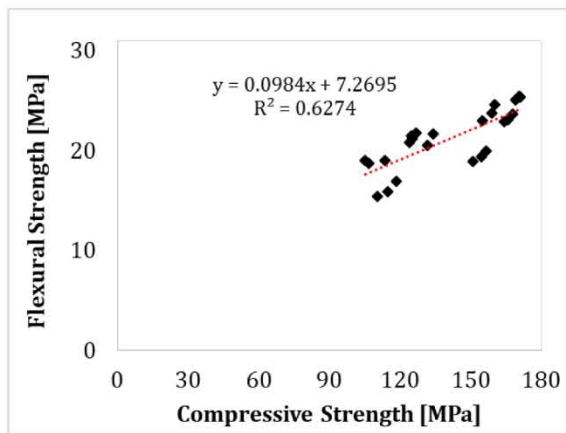**Fig. 12.** Load-deflection curves of the final mixes.

Fig. 13. Correlation of compressive strength and flexural tensile strength (final mixes).

the fact that cement quality and w/c ratio do not influence the flexural tensile strength as much as compressive strength. In UHPC having sufficiently strong fiber reinforcement, the effect of the fibers can be determining factor in terms of flexural strength rather than the other factors [53].

4.3. Stress-Strain curves of the specimens under compression loading

Stress–strain curves obtained from the UHPC series can be found in Fig. 14. Modulus of elasticity (E_c) values calculated by using Eq. (3) can be found in Table 9.

During the experiment, after 90% of the peak loads were exceeded, some strain gauges were damaged together with the concrete (Fig. 15). Thus data could not be collected from strain gauges when approaching the ultimate load value in some specimens. However, this circumstance does not constitute an obstacle in determining the modulus of elasticity (see Equation (3)).

In particular, the series containing crushed quartz sand exhibited much more brittle and rigid behaviour than the series containing natural silica sand. This situation was clearly observed during the experiment, and it was observed that the concrete was damaged by the detaching of a part from the surface with the increase of the load (Fig. 15). In series with the same aggregate type, the modulus of elasticity regularly increased with the increase in compressive strength. However, it was observed that the series containing crushed quartz sand, despite the lower compressive strength, had a higher modulus of elasticity than the series using natural silica sand (see Table 7 and Table 9). In UHPC containing natural silica sand, a modulus of elasticity similar to that of crushed quartz sand mixes (IM-C-WT and IM-D-WT) was only reached with the higher compressive strengths obtained by optimising the mix (i.
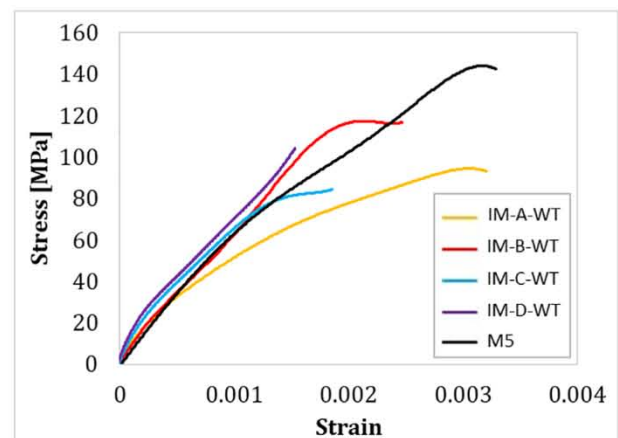

Fig. 14. Stress–strain curves of cylindrical specimens under compression loading.

Table 9
Modulus of elasticity values.

Concrete Series	IM-A-WT	IM-B-WT	IM-C-WT	IM-D-WT	M5
E_c [GPa]	52.7	54.4	61.8	63.7	62.5

Fig. 15. View of the specimens after compression test.

e. M5). For instance, in the case of using natural silica sand, a compressive strength approximately 40% greater than the series containing crushed quartz sand was required in order to obtain a similar modulus of elasticity. In another study conducted by Pourbaba et al. [25], although a strength similar to that achieved in this study (i.e. ~ 140 MPa for cylindrical specimen) was achieved by increasing the fiber content to 6% (by weight), lower modulus of elasticity values were reported. However, it is observed that the modulus of elasticity values found in this study are in agreement with Shafieifar et al. [56]. They reported modulus of elasticity as 60 GPa for 138 MPa of compressive strength.

The modulus of elasticity value of the M5 series with the highest compressive strength was 62.5 GPa. Thus, M5 had a modulus of elasticity approximately 15% greater than IM-B-WT (i.e. E_c = 54.4 GPa) having the same type of aggregate and fiber content. This resulted from the increase of compressive strength owing to optimisation steps, such as the reduction of the w/c ratio, the use of high strength cement and the optimisation of aggregate granulometry. When the fiber volume increased, the modulus of elasticity increased. This finding is confirmed by Pourbaba et al. [25]. Increases in compressive strength arising from the increase in fiber content led to increase in modulus of elasticity. The relationship between compressive strength and modulus of elasticity was shown in Fig. 16. Fiber inclusion may generally reduce the modulus of elasticity in conventional concrete [50]. However, due to the fact that short fibers act as a rigid aggregate, the modulus of elasticity values in UHPC do not decrease, but rather increase related to the increased compressive strength [13]. Although the correlation coefficient is lower due to the smaller number of specimens containing crushed quartz sand (specimens from only IM-C and IM-D series), a considerably high correlation was obtained in particular for UHPC containing natural silica sand (i.e. R^2 = 0.89).

Various equations are available in the literature to calculate the modulus of elasticity depending on the compressive strength of UHPC [57–61]. Ma et al. [57] proposed Equation (5) to determine the modulus of elasticity of UHPC without coarse aggregate and compared the proposed equation with the CEB-FIP Model Code [62]. The coefficient k, given as 21,500 in [62], was revised by [57] as 19000.
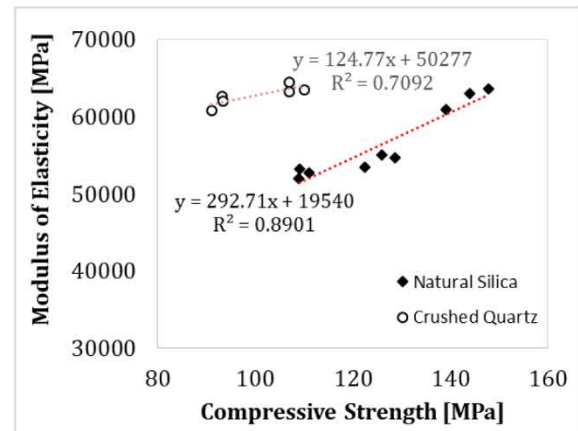

Fig. 16. Correlation of compressive strength and modulus of elasticity.

$$E_c = k\left(\frac{f_c}{10}\right)^{\frac{1}{3}} \tag{5}$$

Federal Highway Administration (FHWA) [58] recommended Equation (6) for determining the modulus of elasticity, in the technical report named FHWA-HRT-14–084. According to Equation (6), f_c should be taken in ksi.

$$E_c = 1550\sqrt{f_c} \tag{6}$$

Equation (7) was taken from AFGC 2013 [59]. Additionally, it is stated that the k value in the equation varies 8800 and 11000 for various UHPC mixtures. Equation (8) and Equation (9) were taken from [60] and [61], respectively.

$$E_c = k(f_c)^{\frac{1}{3}} \tag{7}$$

$$E_c = 11800(f_c)^{\frac{1}{3.14}} \tag{8}$$

$$E_c = 8010(f_c)^{0.36} \tag{9}$$

where f_c represents compressive strength, and k is the factor that links the compressive strength to the modulus of elasticity, depending on the type of aggregate.

Considering the experimental results, it was seen that the k coefficient given in Equation (7) should be 13,500 and 11200, respectively, for the UHPC mixtures with crushed quartz sand and natural silica sand investigated in this study. Likewise, in the case the coefficient k in Equation (5) is taken as 29,000 and 24000, respectively for crushed quartz sand and natural silica sand, the equation seems more compatible with the experimental results. The comparison of the results obtained using these generated coefficients with the equations in the literature and experimental results are provided in Table 10. While the modulus of elasticity values of the crushed quartz sand series differ from the equations due to their lower compressive strength but higher modulus of elasticity, modulus of elasticity values of the series containing natural silica sand stayed in the range (close to the higher bound of the range) specified in [59]. However, it was observed that the modulus of elasticity of the UHPC mixtures investigated in this study could be predicted more accurately by means of the revised new k coefficients.

4.4. Flexural, splitting and Pull-out behaviour of the optimised mix

In this section, the flexural behaviour of M5, which is the final mix achieved by optimising, was examined in detail. The load–deflection graph obtained from the $100 \times 100 \times 400$ mm prism specimens is shown in Fig. 17. Toughness indices and residual strength factors were determined according to ASTM standard [63] and provided in Table 11.

Table 10
Comparison of modulus of elasticity values (in GPa).

	Experiment series	Ma et al. [57]	FHWA-HRT-14-084 [58]	AFGC 2013 [59]	Kollmorgen [60]	Alsalman [61]	Proposed equation in this study	Experimental
UHPC mixes with natural silica sand	IM-A-WT	42.2	42.6	42.1–52.7	52.7	43.5	53.3	52.7
	IM-B-WT	44.2	45.6	44.1–55.1	55.0	45.6	55.8	54.4
	M5	46.2	48.7	46.1–57.6	57.4	47.9	58.3	62.5
UHPC mixes with crushed quartz sand	IM-C-WT	39.9	39.2	39.8–49.8	49.9	40.9	60.9	61.8
	IM-D-WT	42.0	42.3	41.9–52.4	52.4	43.2	64.1	63.7
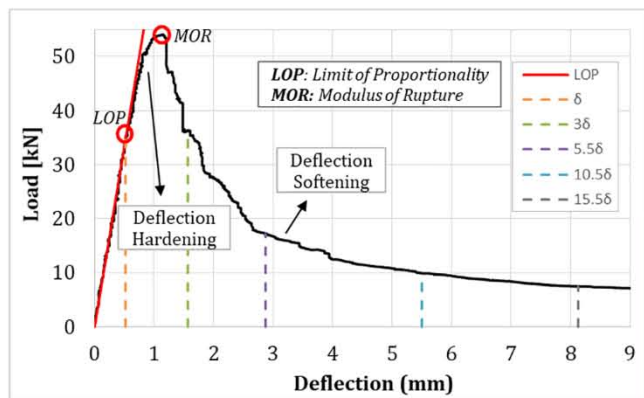
Fig. 17. Load-deflection curve of the M5.

Toughness indices I_5, I_{10}, I_{20} and I_{30} were calculated by dividing the area up to a deflection of 3, 5.5, 10.5, 15.5 times the first crack deflection (δ) by the area up to first crack, respectively. First crack was observed at the point where the linearity ended (LOP) in the load–deflection curve, as also confirmed by [54]. Residual strength factors (denoted as $R_{5,10}$, $R_{10,20}$ and $R_{20,30}$) represent the remaining strength in fiber-reinforced concrete derived from the toughness indices [64] and were calculated as presented in Equation (10).

$$R_{M,N} = C(I_N - I_M) \tag{10}$$

where I_N and I_M are the toughness indices (N > M), and constant C equals to 100/(N-M).

During the experiments, although the first audible sizzling sound, corresponding to a few fibers being pulled out from the matrix, was heard under approximately 20 kN load, the first crack occurred under 35 kN load. In UHPC, cracks are halted by short fibers as soon as they start to form [26]. Despite debonding of a few fibers, the fact that a distinct crack did not occur immediately is thought to be due to the presence of a considerable amount of short fibers in the mix. In other words, the high number of fibers per unit volume had an effect on this circumstance. Load continued to be applied and the maximum load value that was carried by the specimens is determined to be approximately 54 kN. Average flexural tensile strength was calculated as 16.22 MPa depending on the maximum load value of the test specimens under bending. After the first crack is formed, longer fibers played an active role in

controlling the larger cracks and increased the final strength [65]. Moreover, in addition to high compressive and tensile strength, UHPC is expressed by multiple micro-cracks and deflection hardening behaviour [52,54,55]. As seen in Fig. 17, although the first crack was observed at a load of 35 kN, the specimen could continue to carry more load. In other words, the specimen continued to carry a load up to 1.5 times the load value at which crack formation was first seen, thus both the deflection hardening and deflection softening stages were observed (Fig. 17). While the toughness value of the sample was 9 kN.mm until the first crack was formed, it had more than 4 times toughness (i.e. 37.95 kN. mm) when it reached the peak load. At the end of the experiment, the area under the curve exceeded 16 times the area at the time of the first crack (i.e. $I_{30} = 16.15$). Moreover, it was observed that even if the deflection at the time of the first crack reaches 3 times, specimens can still carry 67% of the maximum load.

When the specimen size increased, the flexural tensile strength decreased. This is in agreement with the findings in the literature [29,43]. In the case of increasing the specimen size (i.e. from 40 × 40 × 160 mm to 150 × 150 × 750 mm), the decrease in flexural tensile strength obtained might be up to 40% [53]. In this study, the flexural tensile strength obtained from the 100 × 100 × 400 mm prism specimen was 16.22 MPa, while approximately 56% greater (i.e. 25.29 MPa) flexural tensile strength was obtained from 50 × 50 × 300 mm specimen manufactured from the same mix (i.e. Mix # 5). The higher strength obtained from the small size specimens is based on the surface layer size effect. Due to the fact that random fiber orientation is restricted close to the surface of the mold, fibers on the molded surface tend to align parallel to the mold surface. Therefore, fibers can have an advantage in bridging the cracks that form in the perpendicular direction. Strength of the surface layer of the specimen becomes greater than the inside. Since the surface layer constitutes a larger part of the total cross-sectional area, small-sized specimens have a higher flexural strength [43]. Besides, according to Weibull's theory, specimens can be modeled as a chain with many elements. Since a larger specimen has more elements in the chain, the failure probability is higher than that of the smaller specimen [29].

Splitting tensile test setup is illustrated in Fig. 18a while the appearance of the specimen after the experiment is shown in Fig. 18b. All specimens showed a ductile failure mode due to their high fiber content, did not split into two pieces, and remained intact. The crack formed parallel to the loading plane and almost linearly along the midline as seen in Fig. 18b. Average splitting tensile strength value for the optimised final mix (M5) were 18.95 MPa. This value seems greater than the values reported by [66–68]. This is thought to be due to the
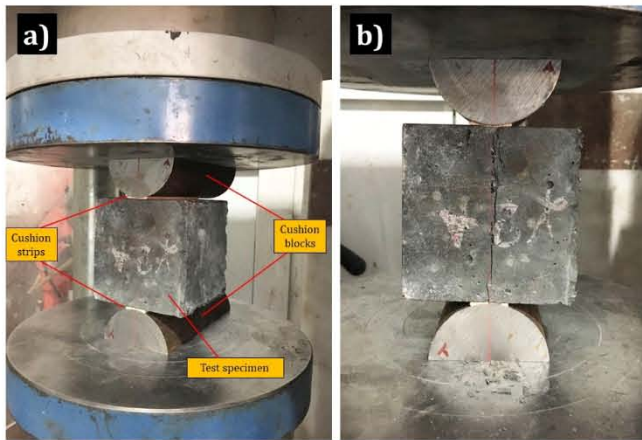
Table 11
Toughness indices and residual strength factors of the M5.

	Deflection	P (kN)	δ (mm)	f (MPa)	Toughness (kN.mm)	Toughness Indices		Residual Strength Factors	
	δ	35.00	0.52	10.50	9.07				
	MOR	54.05	1.13	16.22	37.95				
Residual Strengths	3δ	36.30	1.57	10.89	57.07	I5	6.29		
	5.5δ	17.25	2.88	5.18	90.16	I10	9.94	R5,10	72.97
	10.5δ	9.89	5.50	2.97	124.14	I20	13.69	R10,20	37.46
	15.5δ	7.44	8.12	2.23	146.52	I30	16.15	R20,30	24.67

Fig. 18. Splitting tensile test (a) test setup (b) failure mode of the specimen.

Fig. 20. Load-displacement curve in the pull-out test.

strong bond between fiber and matrix. Splitting tensile strength in fiber-reinforced concretes is directly related to adherence between the fiber and the matrix. The pull-out test to demonstrate the adherence of the fibers is shown in Fig. 19. As a result of the pull-out test, it was observed that the fibers did not slip from the matrix and ruptured (Fig. 19c). This indicates sufficient bonding performance of the steel fiber in the UHPC matrix. Moreover, the load–displacement graph obtained from the pull-out experiment is shown in Fig. 20. Additionally, it should be noted that a little spalling in the matrix was initially observed during the pull-out experiment (Fig. 19b). A slight movement in the steel fiber under pull-out load caused this spalling. Despite a slight movement in the steel fiber, it is thought that the microfibers resist this movement and prevent the steel fiber from tear out the matrix, and thus the adherence continues, as also seen in Fig. 20. Hence, excellent fiber–matrix bond was obtained, the steel fiber was held very strongly by the matrix and broke without considerable damage to the matrix.

5. Conclusion

In this study, mixture optimisation was the goal in order to obtain a UHPC that can be used in structural applications. Therefore, many parameters such as fiber content, aggregate type, cement type, curing method, compaction method, aggregate granulometry, water to cement ratio were examined. The following conclusions are drawn from this study:

- UHPC with a compressive strength of 170 MPa that has excellent workability was developed under standard water curing.
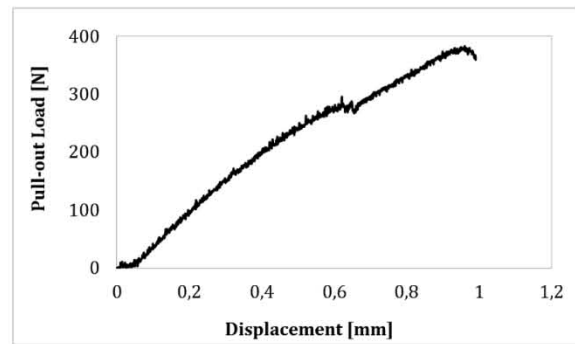
- In cases where heat treatment is not available, a well-flowable UHPC that meets the required strength criteria and can also be used in structural applications can be manufactured by means of water curing to be applied properly instead of heat treatment. However, the choice of the appropriate compaction method, fiber content, cement type and w/c ratio together with the optimisation of aggregate granulometry is also of great importance.
- Fiber inclusion improves the mechanical properties. In addition to increasing the total fiber volume from 2% to 3%, the combination of short fiber and long fiber positively affected the flexural strength, post-peak ductility and toughness properties. The conversion of fiber reinforcement from 2% short straight fiber reinforcement to 3% hybrid fiber reinforcement led to increases up to 16% and 48%, respectively in compressive strength and flexural strength.
- Specimen type (cube or cylinder) had no significant effect on the percentage of increase in compressive strength arising from the fiber content. When the fiber content increased, the compressive strength increased almost at the same rate in cylinder and cube specimens.
- Wet hessian application reduced both compressive strength and flexural tensile strength, compared to standard water curing. Loss of strength was more remarkable in UHPC series having high fiber volume. In the case of wet hessian curing application, the fiber content did not contribute to the compressive and flexural strength as much as it did in the water cured specimens.
- Use of natural silica sand led to much better results in UHPC compared to crushed quartz sand, in terms of mechanical properties. Remarkable increases in compressive and flexural strength was observed when using natural silica sand. The proper choice of aggregate type had a positive effect in terms of ductility as well as strength.
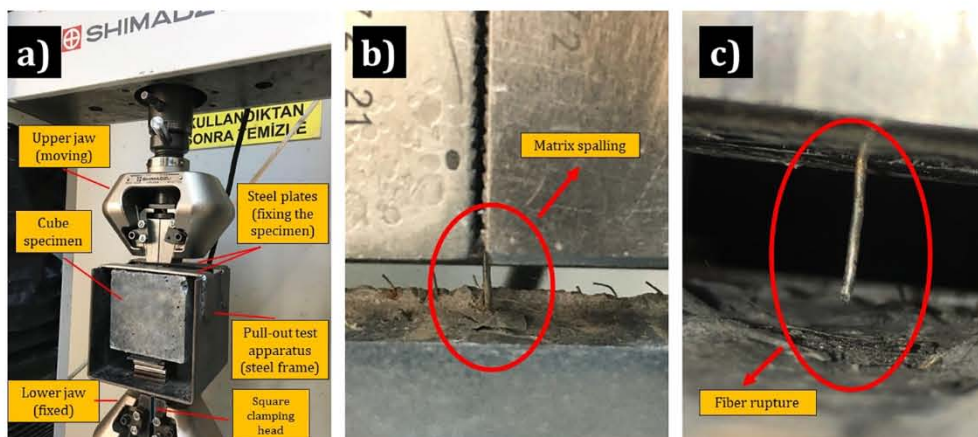

Fig. 19. Pull-out test (a) test apparatus (b) during the experiment (c) after the experiment.

- Modulus of elasticity values changed depending on compressive strength. Since the compressive strength increases when the fiber content increases, the modulus of elasticity also increased.
- Experimentally obtained modulus of elasticity values were predicted accurately, using the new *k* coefficients determined to predict the modulus of elasticity.
- When the w/c ratio was decreased by 0.01, the compressive strength increased by only 5%. The increase was 17% when the cement type was also changed in addition to the 0.01 decrease in the water to cement ratio.
- The air voids on the specimen surfaces are effective on compressive strength. Even if they are not completely eliminated, reduction of their diameter and the number led to a significant increase in compressive strength.
- It is difficult for the fibers to be pulled out from a high-strength matrix with high compactness. Therefore, the flexural and splitting tensile strength increased due to the excellent matrix-fiber bond and increased efficiency of the fibers in the matrix obtained as a result of optimisation of aggregate granulometry.
- A considerably strong linear relationship was found between the compressive and flexural strengths of the UHPC series having the same cement type. Contrary to conventional concretes, the significant contribution of fibers to compressive strength became effective in this situation.
- When the specimen size increased, the flexural tensile strength decreased. Due to the high probability of defects in the large size specimen and the notch effect, approximately 56% greater flexural tensile strength was obtained in the small size prism specimen.

CRediT authorship contribution statement

Kutalmış Recep Akça: Investigation, Writing – original draft, Writing – review & editing. **Metin İpek:** Investigation, Writing – original draft, Writing – review & editing.

Declaration of Competing Interest

The authors declare that they have no known competing financial interests or personal relationships that could have appeared to influence the work reported in this paper.

References

[1] Annex U of CSA-A23.1, Ultra-High-Performance Concrete, Canadian Standards Association (2019).
[2] ASTM C1856, Standard Practice for Fabricating and Testing Specimens of Ultra-High Performance Concrete, ASTM Int. (2017).
[3] GB/T 31387, Reactive powder concrete, Standardization Administration of the PRC, (2015).
[4] NF P 18-470, Concrete — Ultra-high performance fibre-reinforced concrete — Specifications, performance, production and conformity, Association Francaise de Normalisation (AFNOR) (2016).
[5] C.M. Tam, V.W.Y. Tam, K.M. Ng, Assessing drying shrinkage and water permeability of reactive powder concrete produced in Hong Kong, Constr. Build. Mater. 26 (1) (2012) 79–89, https://doi.org/10.1016/j.conbuildmat.2011.05.006.
[6] D. Wang, C. Shi, Z. Wu, J. Xiao, Z. Huang, Z. Fang, A review on ultra high performance concrete: Part II. Hydration, microstructure and properties, Constr. Build. Mater. 96 (2015) 368–377, https://doi.org/10.1016/j.conbuildmat.2015.08.095.
[7] D. Corvez, B. Masson, UHPFRC solutions for the retrofit of nuclear reactor containment walls, Proc. of Int. Symp. on Ultra High Performance Fiber-Reinforced Concrete (2013) 147–156.
[8] T.T. Ngo, D.J. Kim, J.H. Moon, S.W. Kim, Strain rate-dependent shear failure surfaces of ultra-high-performance fiber-reinforced concretes, Constr. Build. Mater. 171 (2018) 901–912, https://doi.org/10.1016/j.conbuildmat.2018.03.180.
[9] M. Vigneshwari, K. Arunachalam, A. Angayarkanni, Replacement of silica fume with thermally treated rice husk ash in Reactive Powder Concrete, J. Clean. Prod. 188 (2018) 264–277, https://doi.org/10.1016/j.jclepro.2018.04.008.
[10] Y.L. Voo, S.J. Foster, R.I. Gilbert, Shear strength of fiber reinforced reactive powder concrete prestressed girders without stirrups, J. Adv. Concr. Technol. 4 (1) (2006) 123–132, https://doi.org/10.3151/jact.4.123.
[11] F. Baby, P. Marchand, F. Toutlemonde, Shear Behavior of Ultrahigh Performance Fiber-Reinforced Concrete Beams. I: Experimental Investigation, J. Struct. Eng. 140 (5) (2014) 04013111, https://doi.org/10.1061/(ASCE)ST.1943-541X.0000907.
[12] P.S. Dong, N. Van Tuan, L.T. Thanh, N.C. Thang, V.H. Cu, J.H. Mun, Compressive strength development of high-volume fly ash ultrahigh-performance concrete under heat curing condition with time, Appl. Sci. 10 (2020) 1–18, https://doi.org/10.3390/app10207107.
[13] M. Ipek, K. Yilmaz, M. Sümer, M. Saribiyik, Effect of pre-setting pressure applied to mechanical behaviours of reactive powder concrete during setting phase, Constr. Build. Mater. 25 (1) (2011) 61–68, https://doi.org/10.1016/j.conbuildmat.2010.06.056.
[14] P. Richard, M. Cheyrezy, Composition of reactive powder concretes, Cem. Concr. Res. 25 (7) (1995) 1501–1511, https://doi.org/10.1016/0008-8846(95)00144-2.
[15] N.M. Azmee, N. Shafiq, Ultra-high performance concrete: From fundamental to applications, Case Stud. Constr. Mater. 9 (2018) e00197, https://doi.org/10.1016/j.cscm.2018.e00197.
[16] P.u. Zhang, Y. Huang, Y. Li, J. Zhao, H. Dong, T. Chen, Influence Factors on the Properties of Ultrahigh-Performance Fiber-Reinforced Concrete Cured under the Condition of Room Temperature, Advances in Civil Engineering 2018 (2018) 1–9, https://doi.org/10.1155/2018/2754735.
[17] B.A. Graybeal, Compressive behavior of ultra-high-performance fiber-reinforced concrete, ACI Mater. J. 104 (2007) 146–152, https://doi.org/10.14359/18577.
[18] Y.e. Shi, G. Long, X. Zen, Y. Xie, T. Shang, Design of binder system of eco-efficient UHPC based on physical packing and chemical effect optimization, Constr. Build. Mater. 274 (2021) 121382, https://doi.org/10.1016/j.conbuildmat.2020.121382.
[19] M. Chen, W. Zheng, A study on optimum mixture ratio of reactive powder concrete, Adv. Mater. Sci. Eng. 2018 (2018) 1–7, https://doi.org/10.1155/2018/7196873.
[20] H. Yiğiter, S. Aydın, H. Yazıcı, M.Y. Yardımcı, Mechanical performance of low cement reactive powder concrete (LCRPC), Compos. Part B Eng. 43 (8) (2012) 2907–2914, https://doi.org/10.1016/j.compositesb.2012.07.042.
[21] S. Nasrin, A. Ibrahim, Flexural response of Ultra-High-Performance Concrete (UHPC) hybrid bridge deck connections made with local materials, Constr. Build. Mater. 270 (2021) 121451, https://doi.org/10.1016/j.conbuildmat.2020.121451.
[22] S. Kazemi, A.S. Lubell, Influence of Specimen Size and Fiber Content on Mechanical Properties of Ultra-High-Performance Fiber-Reinforced Concrete, ACI Mater. J. 109 (2012).
[23] F. Dingqiang, R. Yu, L. Kangning, T. Junhui, S. Zhonghe, W.u. Chunfeng, W. Shuo, G. Zhenfeng, H.u. Zhengdong, S.u. Qiqi, Optimized design of steel fibres reinforced ultra-high performance concrete (UHPC) composites: Towards to dense structure and efficient fibre application, Constr. Build. Mater. 273 (2021) 121698, https://doi.org/10.1016/j.conbuildmat.2020.121698.
[24] G.D. Ashkezari, F. Fotouhi, M. Razmara, Experimental relationships between steel fiber volume fraction and mechanical properties of ultra-high performance fiber-reinforced concrete, J. Build. Eng. 32 (2020) 101613, https://doi.org/10.1016/j.jobe.2020.101613.
[25] M. Pourbaba, E. Asefi, H. Sadaghian, A. Mirmiran, Effect of age on the compressive strength of ultra-high-performance fiber-reinforced concrete, Constr. Build. Mater. 175 (2018) 402–410, https://doi.org/10.1016/j.conbuildmat.2018.04.203.
[26] I. Markovic, High-Performance Hybrid-Fibre Concrete – Development and Utilisation, Dissertation, Delft University of Technology, DPU Science, Delft University Press, 2006.
[27] G.S. Ryu, S.T. Kang, J.J. Park, K.T. Koh, S.W. Kim, Mechanical behavior of UHPC (ultra high performance concrete) according to hybrid use of steel fibers, Adv. Mater. Res. 287–290 (2011) 453–457, https://doi.org/10.4028/www.scientific.net/AMR.287-290.453.
[28] H. Huang, X. Gao, K.H. Khayat, A. Su, Influence of fiber alignment and length on flexural properties of UHPC, Constr. Build. Mater. 290 (2021) 122863, https://doi.org/10.1016/j.conbuildmat.2021.122863.
[29] D.L. Nguyen, D.J. Kim, G.S. Ryu, K.T. Koh, Size effect on flexural behavior of ultra-high-performance hybrid fiber-reinforced concrete, Compos. Part B Eng. 45 (1) (2013) 1104–1116, https://doi.org/10.1016/j.compositesb.2012.07.012.
[30] S. Platias, K.I. Vatalis, G. Charalampides, Suitability of Quartz Sands for Different Industrial Applications, Procedia Econ. Financ. 14 (2014) 491–498, https://doi.org/10.1016/s2212-5671(14)00738-2.
[31] H.J. Chen, Y.L. Yu, C.W. Tang, Mechanical properties of ultra-high performance concrete before and after exposure to high temperatures, Materials. 13 (2020) 1–17, https://doi.org/10.3390/ma13030770.
[32] Y.L. Voo, W.K. Poon, S.J. Foster, Shear Strength of Steel Fiber-Reinforced Ultrahigh-Performance Concrete Beams without Stirrups, J. Struct. Eng. 136 (11) (2010) 1393–1400, https://doi.org/10.1061/(ASCE)ST.1943-541X.0000234.
[33] Z. Wu, C. Shi, W. He, Comparative study on flexural properties of ultra-high performance concrete with supplementary cementitious materials under different

curing regimes, Constr. Build. Mater. 136 (2017) 307–313, https://doi.org/10.1016/j.conbuildmat.2017.01.052.

[34] EN 12390-2, Testing Hardened Concrete – Part 2: Making and Curing Specimens for Strength Tests, European Committee for Standardization, (2009).

[35] W.B. Fuller, S.E. Thompson, The laws of proportioning concrete, ASCE J. Transport 59 (1907) 67–143.

[36] M. Ipek, K. Yilmaz, M. Uysal, The effect of pre-setting pressure applied flexural strength and fracture toughness of reactive powder concrete during the setting phase, 26 (2012) 459–465. https://doi.org/10.1016/j.conbuildmat.2011.06.045.

[37] ASTM C1437, Standard Test Method for Flow of Hydraulic Cement Mortar, ASTM International, 2007.

[38] S.H. Lee, S. Kim, D.Y. Yoo, Hybrid effects of steel fiber and carbon nanotube on self-sensing capability of ultra-high-performance concrete, Constr. Build. Mater. 185 (2018) 530–544, https://doi.org/10.1016/j.conbuildmat.2018.07.071.

[39] K. Wille, A. Naaman, G. Parra-Montesinos, Ultra-High Performance Concrete with Compressive Strength Exceeding 150 MPa (22 ksi): A Simpler Way, Aci Materials Journal 108 (2011) 46–54, https://doi.org/10.14359/51664215.

[40] K.Q. Yu, J.T. Yu, J.G. Dai, Z.D. Lu, S.P. Shah, Development of ultra-high performance engineered cementitious composites using polyethylene (PE) fibers, Constr. Build. Mater. 158 (2018) 217–227, https://doi.org/10.1016/j.conbuildmat.2017.10.040.

[41] ASTM C469 C469M, Standard Test Method for Static Modulus of Elasticity and Poisson's Ratio of Concrete in Compression ASTM Int. 2014 1 5.

[42] ASTM C348, Standard Test Method For Flexural Strength of Hydraulic-Cement Mortars, ASTM Int. (2014).

[43] J. Fládr, P. Bílý, Specimen size e ff ect on compressive and fl exural strength of high-strength fi bre-reinforced concrete containing coarse aggregate, Compos. Part B 138 (2018) 77–86, https://doi.org/10.1016/j.compositesb.2017.11.032.

[44] B. He, X. Zhu, Q. Ren, Z. Jiang, Effects of fibers on flexural strength of ultra-high-performance concrete subjected to cryogenic attack, Constr. Build. Mater. 265 (2020) 120323, https://doi.org/10.1016/j.conbuildmat.2020.120323.

[45] H.-O. Shin, S.-J. Lee, D.-Y. Yoo, Bond Behavior of Pretensioned Strand Embedded in Ultra-High-Performance Fiber-Reinforced Concrete, Int. J. Concr. Struct. Mater. 12 (1) (2018), https://doi.org/10.1186/s40069-018-0249-4.

[46] D.Y. Yoo, N. Banthia, Y.S. Yoon, Predicting the flexural behavior of ultra-high-performance fiber-reinforced concrete, Cem. Concr. Compos. 74 (2016) 71–87, https://doi.org/10.1016/j.cemconcomp.2016.09.005.

[47] GB/T 50081, Standard for Test Method of Mechanical Properties of Ordinary Concrete (Section 9: Test of splitting tensile strength), China Architecture & Building Press, 2019.

[48] S. Feng, H. Xiao, H. Li, Comparative studies of the effect of ultrahigh-performance concrete and normal concrete as repair materials on interfacial bond properties and microstructure, Eng. Struct. 222 (2020) 111122, https://doi.org/10.1016/j.engstruct.2020.111122.

[49] Y. Ju, T. Shen, D. Wang, Bonding behavior between reactive powder concrete and normal strength concrete, Constr. Build. Mater. 242 (2020) 118024, https://doi.org/10.1016/j.conbuildmat.2020.118024.

[50] K.R. Akça, Ö. Çakır, M. İpek, Properties of polypropylene fiber reinforced concrete using recycled aggregates, Constr. Build. Mater. 98 (2015) 620–630, https://doi.org/10.1016/j.conbuildmat.2015.08.133.

[51] C. Ţibea, D.V. Bompa, Ultimate shear response of ultra-high-performance steel fibre-reinforced concrete elements, Arch. Civ. Mech. Eng. 20 (2020) 1–16, https://doi.org/10.1007/s43452-020-00051-z.

[52] T. Leutbecher, J. Rebling, Predicting the postcracking strength of ultra-high performance fiber reinforced concrete by means of three-point bending tests according to EN 14651, Struct. Concr. 20 (6) (2019) 2081–2095, https://doi.org/10.1002/suco.v20.610.1002/suco.201900070.

[53] E. Fehling, M. Schmidt, J. Walraven, T. Leutbecher, S. Fröhlich, Ultra-High Performance Concrete UHPC Fundamentals – Design – Examples, Ernst&Sohn (A Wiley Brand), Berlin (2014) 1–189.

[54] D.Y. Yoo, S.T. Kang, Y.S. Yoon, Enhancing the flexural performance of ultra-high-performance concrete using long steel fibers, Compos. Struct. 147 (2016) 220–230, https://doi.org/10.1016/j.compstruct.2016.03.032.

[55] P. Máca, R. Sovják, T. Vavřiník, Experimental investigation of mechanical properties of UHPFRC, Procedia Eng. 65 (2013) 14–19, https://doi.org/10.1016/j.proeng.2013.09.004.

[56] M. Shafieifar, M. Farzad, A. Azizinamini, Experimental and numerical study on mechanical properties of Ultra High Performance Concrete (UHPC), Constr. Build. Mater. 156 (2017) 402–411, https://doi.org/10.1016/j.conbuildmat.2017.08.170.

[57] J. Ma F. Dehn N.V. Tue M. Orgass D. Schmidt Comparative Investigations on Ultra-High Performance Concrete with and without Coarse Aggregates 2004 Kassel, Germany, Sept 205 212.

[58] B. Graybeal, Design and Construction of Field-Cast UHPC Connections, Federal Highway Administration Publication No. FHWA-HRT-14-084 (2014).

[59] AFGC, Bétons fibrés à ultra-hautes performances (Ultra high performance fibre reinforced concretes)-Recommandations, (2013).

[60] G.A. Kollmorgen, Impact of age and size on the mechanical behavior of an ultra high performance concrete (Doctoral dissertation), Michigan Technological University, 2004.

[61] A. Alsalman, C.N. Dang, G.S. Prinz, W.M. Hale, Evaluation of modulus of elasticity of ultra-high performance concrete, Constr. Build. Mater. 153 (2017) 918–928.

[62] CEB-FIP-Model-Code 1990, Design of concrete structures, Comité Euro-International du Beton, (1993).

[63] ASTM C1018-97, Standard Test Method for Flexural Toughness and First-Crack Strength of Fiber-Reinforced Concrete (Using Beam With Third-Point Loading), ASTM Stand. (1997).

[64] A.J. Hamad, R.J.A. Sldozian, Flexural and Flexural Toughness of Fiber Reinforced Concrete-American Standard Specifications Review, GRD J.-Global Res. Dev. J. Eng. 4 (3) (2019) 5–13.

[65] H.R. Pakravan, M. Latifi, M. Jamshidi, Hybrid short fiber reinforcement system in concrete: A review, Constr. Build. Mater. 142 (2017) 280–294, https://doi.org/10.1016/j.conbuildmat.2017.03.059.

[66] A. Hasnat, N. Ghafoori, Properties of ultra-high performance concrete using optimization of traditional aggregates and pozzolans, Constr. Build. Mater. 299 (2021) 123907, https://doi.org/10.1016/j.conbuildmat.2021.123907.

[67] R. Karim, M. Najimi, B. Shafei, Assessment of transport properties, volume stability, and frost resistance of non-proprietary ultra-high performance concrete, Constr. Build. Mater. 227 (2019) 117031, https://doi.org/10.1016/j.conbuildmat.2019.117031.

[68] W. Meng, M. Valipour, K.H. Khayat, Optimization and performance of cost-effective ultra-high performance concrete, Mater. Struct. Constr. 50 (2017) 1–16, https://doi.org/10.1617/s11527-016-0896-3.